Recruitment of Both Uniform and Differential Binding Energy in Enzymatic Catalysis: Xylanases from Families 10 and 11[†]

Jacqueline Wicki, Johann Schloegl,[‡] Chris A. Tarling, and Stephen G. Withers*

Department of Chemistry, University of British Columbia, 2036 Main Mall, Vancouver, British Columbia, Canada V6T 1Z1

Received February 21, 2007; Revised Manuscript Received April 4, 2007

ABSTRACT: The contributions of enzyme−substrate hydrogen-binding interactions to catalysis by two different families of xylanases were evaluated through kinetic studies with two representative wild-type enzymes, *Cellulomonas fimi* xylanase (Cex) and *Bacillus circulans* xylanase (Bcx), on a series of monodeoxygenated and monodeoxyfluorinated *p*-nitrophenyl xylobioside substrates. Effects of substitution in the distal (−2 subsite) sugar on k_{cat}/K_m for Cex were moderately large (up to 2.9 kcal mol^{-1}), with no effect seen on k_{cat}. By contrast, substantial effects upon both k_{cat} and k_{cat}/K_m were seen for substrates modified in the proximal (−1 subsite) sugar. Very similar results were obtained with Bcx. Kinetic analyses with a series of eight mutants of Cex in which active site residues interacting with the substrate were mutated yielded complementary insights. Again, interactions with the distal (−2) sugar were seen to contribute substantially to k_{cat}/K_m (up to 3.7 kcal mol^{-1}), thus to the formation of the glycosyl−enzyme intermediate, but not to k_{cat}, thus to the hydrolysis of the glycosyl−enzyme. Interactions with the proximal (−1) sugar are much more significant, contributing up to 6.7 kcal mol^{-1} to both k_{cat}/K_m and k_{cat}. These results together indicate that interactions with the distal sugar maintain similar magnitudes in the transition states for glycosylation and deglycosylation as well as in the glycosyl−enzyme intermediate and can be referred to as "uniform binding interactions" in the parlance of Albery and Knowles (Albery, W. J., and Knowles, J. R. (1976) *Biochemistry 15,* 5631−5640). Interactions with the proximal sugar are considerably stronger at the deglycosylation transition state than in the intermediate, and fall into the category of differential binding interactions. This behavior likely has its origins in the changes in ring conformation of the proximal sugar but not of the distal sugar between the ground state and the reaction transition state. Correlation of these individual interaction energies with the hydrogen-bonding pattern seen in the glycosyl−enzyme intermediate allows for the assignment of hydrogen-bond strengths to each interaction, with good correlation between the two approaches. These findings are relevant to the discussion of remote binding effects upon enzymatic catalysis.

Enzymes owe a large part of their catalytic prowess to the formation of specific hydrogen bonds with their substrates both in the ground state (Michaelis) complex and most importantly at their transition states. Transient interactions of this kind, which are expressed at the transition states, serve to lower the activation barrier for reaction by stabilizing the transition states, as was clearly elucidated by Jencks, who termed this phenomenon the Circe effect (*42*). An understanding of the magnitudes, distributions and polarities of these individual hydrogen bonds at the reaction transition state is thus of particular importance to understanding enzymatic catalysis and specificity. An additional long-standing, but frequently recurring, question is how enzyme−substrate binding interactions that are remote from the active site can significantly contribute to catalysis. Glycosidases are particularly convenient enzymes with which to explore the roles of such hydrogen-bonding interactions because their substrates are highly hydroxylated and thus necessarily engage in multiple hydrogen-bonding interactions. The substrates are also relatively conformationally stable because of their cyclic nature, and the enzymes are themselves well characterized, with three-dimensional structures of representatives of more than 60 families now being available (*2*).

Two principal methods have been employed to evaluate contributions of individual hydrogen bonds to catalysis by glycosidases and related enzymes. One approach involves the synthesis of a series of substrate analogues in which each hydroxyl group is individually replaced by either a hydrogen or fluorine atom, followed by measurement of the kinetic parameters for reaction of each of these substrates with the wild-type enzyme. This provides a measure of the contribution of the set of H-bonds to the hydroxyl group to transition state stabilization. The other approach involves the generation of a series of mutant enzymes in which the active site residues that form these interactions are mutated, followed by measurement of the kinetic parameters of each mutant with the fully hydroxylated substrate (parent substrate). This provides a measure of the total contribution of *all* interactions

[†] This research was funded by the Natural Sciences and Engineering Research Council and the Protein Engineering Network of Centres of Excellence of Canada. J.S. was funded by the Austrian FWF Schrödinger Fellowship. J.W. was supported by a fellowship from the University of British Columbia.

* To whom correspondence should be addressed. Tel: 604-822-3402. Fax: 604-822-8869. E-mail: withers@chem.ubc.ca.

[‡] Current address: Fresenius-Kabi Austria GmbH, Hafnerstrasse 36, A-8055 Graz, Austria.

10.1021/bi700359e CCC: $37.00
Published on Web 05/16/2007

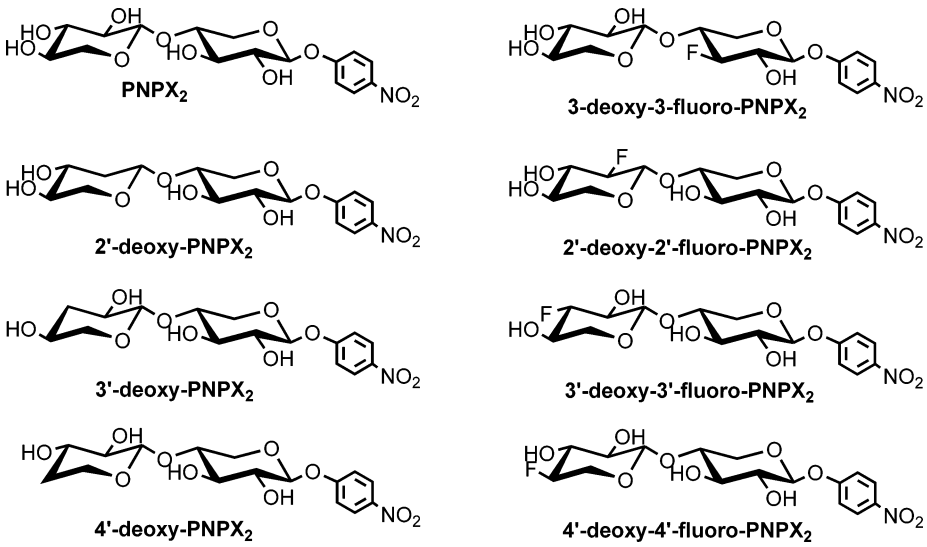

FIGURE 1: Structures of substrates synthesized and subjected to kinetic analysis as substrates for Cex and Bcx.

with that side chain to catalysis. These approaches have been applied to a number of different glycosyl-transferring enzymes, including the β-glucosidases from *Aspergillus wentii* (*3*) and *Agrobacterium* sp. (*4*), *Aspergillus niger* glucoamylase (*5*, *6*), *Escherichia coli* β-galactosidase (*7*), rabbit muscle glycogen phosphorylase (*8*−*10*), and *Schizophyllum commune* trehalose phosphorylase (*11*). These enzymes are all exo-glycosyl transferases that transfer a single sugar residue. Of these, only the study with the *Agrobacterium* sp. β-glucosidase evaluated the contributions of hydrogen binding at each step in catalysis through a combination of steady-state and pre-steady-state kinetic studies.

One of the complications of using deoxygenated and deoxyfluorinated substrates for such an analysis arises from the inductive effects of substituents with vastly different electronegativities and their corresponding effects on the positively charged oxocarbenium ion-like reaction center (*12*). The consequences of these inductive effects are superimposed on the consequences of removal of specific hydrogen bonds; thus, the two effects can be difficult to deconvolute (*3*, *7*, *9*, *13*). However, by an analysis of only kinetic parameters from deoxygenated substrates (where inductive effects will inherently accelerate the reaction), at least a *minimal* estimate of the contributions of hydrogen-bonding interactions at each position can be obtained.

From the study of endo-glycosidases (or exo-glycosidases in which cleavage occurs at least two sugar residues from the chain terminus), it should be possible to evaluate the contributions of hydrogen-binding interactions with the hydroxyl groups on more remote parts of the substrate. This will provide valuable insight into whether and how such interactions help contribute to catalysis, given their remoteness from the reaction center. Such a system has the additional advantage that the interpretation of data from deoxygenated or deoxyfluorinated substrates will not be confused by superimposed inductive effects on the oxocarbenium ion-like transition state, the latter being too far removed to have any significant influence. No such study has, to our knowledge, been performed. The only related study of which we are aware is one on *Bacillus* 1,3-1,4-D-glucan-4-glucanohydrolase (*14*) in which mutagenesis was used to probe presumed hydrogen-bonding interactions in a modeled complex. Once an actual structure of a product complex had been determined, further analysis was performed (*15*).

The two xylanases from *Cellulomonas fimi* (Cex[1], Family 10) and *Bacillus circulans* (Bcx, Family 11) provide ideal systems for such a study. Both are retaining enzymes that follow a two-step, double displacement mechanism involving a covalent glycosyl−enzyme intermediate that is formed and hydrolyzed via oxocarbenium ion-like transition states with acid/base catalytic assistance (*16*). Both enzymes have been characterized structurally by both X-ray crystallography (*17*−*25*) and NMR (*26*−*29*). Extensive kinetic analyses have been performed on the wild-type versions of both enzymes (*19*, *30*−*32*) as well as on mutants in which key catalytic residues have been replaced (*33*−*37*). In this study, we describe the synthesis of a series of deoxy and deoxyfluoro analogues of the substrate *p*-nitrophenyl β-xylobioside (Figure 1) and the kinetic analysis of their reaction with both Cex and Bcx. Furthermore, we describe the generation of eight mutants of Cex in which active-site side chains that interact with the substrate have been mutated and describe the kinetic analysis of the reaction of these mutants with *p*-nitrophenyl β-xylobioside. These results provide new insights into the role of hydrogen binding in catalysis by these two xylanases, in particular, as well as, more generally, into the molecular basis for remote binding effects upon catalysis.

EXPERIMENTAL PROCEDURES

General Methods. Growth media components were obtained from Sigma. Plasmid-containing strains were grown

[1] Abbreviations: Cex, *Cellulomonas fimi* xylanase; Bcx, *Bacillus circulans* xylanase; IPTG, isopropyl β-D-thiogalactoside; BSA, bovine serum albumin; DAST, diethyl amino sulfur trifluoride; $PNPX_2$, *p*-nitrophenyl β-xylobioside; $3F\text{-}PNPX_2$, *p*-nitrophenyl 3-deoxy-3-fluoro-β-xylobioside; $2'H\text{-}PNPX_2$, *p*-nitrophenyl 2′-deoxy-β-xylobioside; $2'F\text{-}PNPX_2$, *p*-nitrophenyl 2′-deoxy-2′-fluoro-β-xylobioside; $3'H\text{-}PNPX_2$, *p*-nitrophenyl 3′-deoxy-β-xylobioside; $3'F\text{-}PNPX_2$, *p*-nitrophenyl 3′-deoxy-3′-fluoro-β-xylobioside; $4'H\text{-}PNPX_2$, *p*-nitrophenyl 4′-deoxy-β-xylobioside; $4'F\text{-}PNPX_2$, *p*-nitrophenyl 4′-deoxy-4′-fluoro-β-xylobioside; 2F-DNPC, 2,4-dinitrophenyl 2-deoxy−2-fluoro-β-cellobioside; DNPC, 2,4-dinitrophenyl β-cellobioside.

in Luria Broth containing 100 μg/mL ampicillin or 50 μg/mL kanamycin. *Pwo* DNA polymerase (originally isolated form the thermophilic archaebacterium *Pyrococcus woesei*) and deoxynucleoside triphosphates were obtained from Roche. *Pfu* DNA polymerase (derived from the thermophilic archaebacterium *Pyrococcus furiosus*) was from Promega. Restriction endonucleases and T4 DNA ligase were from New England BioLabs unless otherwise indicated. *Escherichia coli* One Shot TOP10 competent cells (F^- *mcr*A Δ(*mrr-hsd*RMS-*mcr*BC) ϕ80*lac*ZΔM15 Δ*lac*X74 *deo*R *rec*A1 *ara*D139 Δ(*ara-leu*)7697 *gal*U *gal*K *rps*L *end*A1 *nup*G) and the Zero Blunt PCR Cloning Kit were from Invitrogen. The QuikChange Site-Directed Mutagenesis Kit and Epicurian Coli XL1-Blue electroporation-competent cells (*rec*A1 *end*A1 *gyr*A96 *thi*-1 *hsd*R17 *sup*E44 *rel*A1 *lac* [F′ *pro*AB *lacI*^{q}ZΔM15 Tn10 (Tet^r)]) were from Stratagene. PCR DNA fragment purification and plasmid purification kits were from Qiagen or Promega.

Synthesis of oligonucleotide primers and DNA sequencing were performed by the Nucleic Acids and Peptide Services (NAPS) Unit at the University of British Columbia (Vancouver, Canada). Syntheses of the *p*-nitrophenyl deoxy- and deoxyfluoro-β-xylobiosides, along with full characterizations, are provided as Supporting Information.

Generation of Mutants. The genes encoding for *cex* H80A, H80N, H80Q, K47A, N44A, and E43A were linearly amplified following the protocol outlined in Stratagene's QuikChange Site-Directed Mutagenesis Kit.

The reaction mixture contained 150 ng of oligonucleotide primers, 250 μM each of the four deoxynucleoside triphosphates, and 50 ng of plasmid pUC12-1.1*cex*(PTIS) in 50 μL of *Pfu* DNA polymerase reaction buffer containing 8% DMSO. Plasmid pUC12-1.1*cex*(PTIS) contains the 1.4 kb *cex* gene (*38*). The reaction was initiated by adding 4 U of *Pfu* DNA polymerase (Promega). After heating the reaction mixture to 95 °C for 30 s, 16 cycles (30 s at 95 °C, 1 min at 55 °C, and 9 min at 68 °C) were performed in a thermal cycler (GeneAmp PCR System 2400, Perkin-Elmer). Agarose gel electrophoresis confirmed the presence of sufficient amplification product. The parental supercoiled dsDNA was digested with 20 U of *Dpn* I restriction enzyme at 37 °C for 1 h. Epicurian Coli XL1-Blue electroporation-competent cells (Stratagene) were subsequently transformed with 1 μL of the *Dpn* I treated DNA from the amplification reaction using the BioRad GenePulser II and 0.1 cm cuvettes under the following conditions: 1.8 kV, 25 μF, and 200 Ω. The cells were plated on LB agar plates containing 100 μg/mL ampicillin and incubated at 37 °C overnight. Single colonies were selected and grown overnight in LB media containing 100 μg/mL ampicillin. Plasmid DNA was isolated using the QIAprep Spin Miniprep Kit from Qiagen or the Wizard *Plus* Minipreps DNA Purification System from Promega. Plasmid DNA was stored in water at −20 °C. Restriction endonuclease mapping revealed positive clones, which were subsequently sequenced to verify the correct mutations. The cloned products were subsequently transformed into electrocompetent *E. coli* JM101 cells using the BioRad GenePulser II and 0.2 cm cuvettes under the following conditions: 2.5 kV, 25 μF, and 400 Ω. Cells were selected by the ampicillin resistance conferred by pUC12-1.1 on LB_{amp} agar plates. Single colonies were selected and grown overnight in LB_{amp} for long-term storage in 10% DMSO at −70 °C.

The *E. coli* JM101 transformants from the previously prepared DMSO stocks were selected on LB_{amp} (100 μg/mL) agar plates. A single colony was picked and grown for 6 h in 3 mL of LB_{amp}, and this culture was subsequently used to inoculate 1 L of TYP_{amp}. After the culture grew to an OD_{600} of 2−3 at 30−37 °C, 0.2 mM isopropyl β-D-thiogalactoside (IPTG) was added to induce protein expression and grown for an additional 4 h at 25 °C. Overexpression of the enzyme was monitored by sampling of both induced and non-induced cells using SDS−polyacrylamide gel electrophoresis. Induced cells were then harvested by centrifugation at 5000 rpm for 20 min at 4 °C. A cell extract was prepared using BugBuster Protein Extraction Reagent (Novagen). The cell pellet from a 1 L culture was resuspended in 50 mL of BugBuster reagent at room temperature and 50 μL of Benzonase (Novagen). (Benzonase is a genetically engineered endonuclease from *Serratia marcescens.*) EDTA was added to 0.5 mM and PMSF to 1.0 mM. The mixture was incubated with shaking for 10−20 min. Following removal of the insoluble cell debris by centrifugation at 16,000*g* for 20 min at 4 °C, the soluble cell extract was added to 450 mL of 500 mM NaCl in 50 mM sodium phosphate buffer (pH 7.0). EDTA and PMSF were added to 0.5 mM.

Protein Purification and Characterization. Cex and the mutants of Cex were purified from the clarified cell extract by affinity chromatography on cellulose. Approximately 25 g of CF1 cellulose (Sigma) was gently stirred with distilled water, allowed to settle, and the cellofines were decanted. The cellulose was packed into an XK50/20 column (Pharmacia), yielding a column volume of approximately 150 mL. The column was attached to an FPLC system (Pharmacia) and equilibrated with 5 column volumes of 500 mM NaCl in 50 mM sodium phosphate buffer (pH 7.0) at a flow rate of 5 mL/min. The soluble cell extract from the 1 L cell culture was applied to the column at a flow rate of 5 mL/min. The column was washed with 2 column volumes of 500 mM NaCl in 50 mM sodium phosphate buffer (pH 7.0) followed by 1 column volume of 50 mM sodium phosphate buffer (pH 7.0) at a flow rate of 5 mL/min. Cex protein was eluted with 2.5 column volumes of distilled H_2O at a flow rate of 5 mL/min. The absorbance of the eluate was measured continuously at 280 nm, and appropriate fractions were pooled and passed through a 0.22 μm filter (Millipore).

The protein sample was further purified on a 5 mL HiTrap Mono Q HP column attached to an FPLC system (Pharmacia). The column was washed with 5 column volumes of 20 mM Tris-HCl buffer (pH 7.5), 5 column volumes of 20 mM Tris-HCl buffer containing 1 M NaCl (pH 7.5), and then 10 column volumes of 20 mM Tris-HCl buffer (pH 7.5) at a flow rate of 5 mL/min. The protein sample was adjusted to pH 8.0 with 20 mM Tris-HCl and applied onto the HiTrap Mono Q HP column at a flow rate of 5 mL/min. The column was washed with 4 column volumes of 20 mM Tris-HCl buffer (pH 7.5). Cex protein was eluted from the anion-exchange column with a linear NaCl gradient from 0 to 500 mM in a buffer containing 20 mM Tris-HCl (pH 7.5). Fractions (8 mL) were collected at a flow rate of 5.0 mL/min and analyzed using SDS−polyacrylamide gel electrophoresis on a Mini-PROTEAN II apparatus (BioRad). Protein bands were visualized by staining with Coomassie Blue. Fractions containing pure enzyme were pooled and stored

at 4 °C. If necessary, the enzyme was concentrated to at least 2.0 mg/mL using a Centriprep concentrator (30 kDa cutoff) from Amicon. Final protein concentration was calculated from measured absorbance at 280 nm using the previously determined extinction coefficient for Cex ($\epsilon_{280} = 1.61$ mL mg^{-1} cm^{-1}).

The molecular weights of purified Cex and Cex mutants were determined by ion spray mass spectrometry. Mass spectra were recorded on a PE-Sciex API 300 triple-quadrupole mass spectrometer (Sciex, Thornhill, Ontario, Canada) equipped with an ion spray ion source by Mr. Shouming He. Enzyme samples (10 μg) were injected into the mass spectrometer to generate the spectra. The masses of the generated mutants were confirmed by comparison between the expected molecular weights and those provided by the spectra.

Wild-type Bcx was purified as previously described (*39*). The purified protein ran as a single band on SDS−PAGE with greater than 95% purity by inspection. Mass spectrometric analysis confirmed the molecular mass of the recombinant xylanase and the absence of impurities.

Kinetic Analyses. Michaelis−Menten parameters for aryl glycosides were determined by continuous measurement of the release of the *p*-nitrophenolate using a Unicam UV4 spectrophotometer equipped with a temperature-controlled circulating water bath. The buffer used for Cex was 50 mM sodium phosphate buffer at pH 7.00, containing 0.1% w/v bovine serum albumin (BSA) at 37 °C. The kinetic studies for Bcx were performed at 40 °C in 20 mM MES at pH 6.00, containing 50 mM NaCl and 0.1% w/v BSA. Concentrations of aryl glycosides were confirmed by total hydrolysis of the glycoside and by the determination of the final concentration of *p*-nitrophenolate released. Initial rates of enzyme-catalyzed hydrolysis of aryl glycosides were determined by incubating solutions of the appropriate substrate concentrations in 1 cm cuvettes within the spectrophotometer until thermally equilibrated. Reactions were initiated by the addition of enzyme, and the release of *p*-nitrophenolate was monitored at 400 nm. The concentration of enzyme added and the length of time that the reaction was monitored in each case were selected such that less than 10% of the total substrate was converted to product.

Rates were measured at 8−10 different substrate concentrations ranging from about 0.1 K_m to 7 K_m, where practical. Values for K_m and k_{cat} were determined from the initial rates of hydrolysis (V_0) versus substrate concentration by nonlinear regression analysis using the computer program GraFit 4.0 (*40*). In cases where significant transglycosylation was observed, a nonlinear regression was performed on data from concentrations of 0.1 to approximately 2 times K_m. The values of k_{cat} and K_m so obtained were then compared to those determined from linear regression of the reciprocal data as plotted according to Lineweaver−Burke. In almost all cases, the kinetic constants K_m, V_{max}, and k_{cat} were calculated from a fit to the Michaelis−Menten equation. For those mutants with very high K_m values, for which saturation behavior could not be observed, an accurate value of k_{cat}/K_m was obtained from the slope of the Lineweaver−Burk plot, and approximate estimates of the individual parameters were obtained from the intercepts.

In addition, the second-order rate constants (k_{cat}/K_m) were determined from progress curves at low substrate concentrations using the substrate depletion method as follows. Appropriate substrate at a concentration of less than 1/5 K_m in the appropriate buffer containing 0.1% w/v BSA was incubated until thermally equilibrated. Following the addition of 10 μL enzyme, the release of *p*-nitrophenolate was monitored by following the absorbance at 400 nm until substrate depletion was observed. The change in absorbance with respect to time was fitted to a first-order rate equation using the program GraFit that yielded pseudo-first-order rate constants. At low substrate concentrations, the reaction rates are given by the following equation:

$$V = \left(\frac{k_{cat}}{K_m}\right)[E]_0[S]$$

Thus, pseudo-first-order rate constants measured correspond to $[E]_0(k_{cat}/K_m)$, from which k_{cat}/K_m is easily obtained. The individual contribution of each substrate hydroxyl group to transition-state stabilization with the wild-type enzyme was determined from the relationship $\Delta\Delta G^{\ddagger} = -RT \ln((k_{cat}/K_m)_x/(k_{cat}/K_m)_y)$, where *x* represents a substrate analogue or mutant enzyme and *y* the parent substrate or wild-type enzyme.

RESULTS

Syntheses of the complete set of deoxy and deoxyfluoro analogues of *p*-nitrophenyl β-xylobioside in which the distal sugar was modified were achieved as follows. The protected deoxy or deoxyfluoro xylosides were synthesized via standard synthetic routes involving DAST (diethyl amino sulfur trifluoride) fluorinations and radical deoxygenations. These modified sugars were converted to their corresponding trichloroacetimidates via the hemiacetal, then coupled to *p*-nitrophenyl 2,3-di-*O*-acetyl-β-D-xylopyranoside under boron trifluoride etherate catalysis. Unfortunately, the only substrates that could be prepared in which the proximal xylose residue had been modified were the 2- and 3-fluoro analogues, which were synthesized essentially as described previously (*31*, *41*). All attempts to synthesize the *p*-nitrophenyl 3-deoxy-xylobioside led to decomposition. No attempt was made to synthesize the 2-deoxy analogue because it would be considerably more labile again. Full descriptions of the syntheses and characterizations are provided as Supporting Information.

The residues of Cex to be mutated were chosen on the basis of their active site location and their observed involvement in hydrogen-bonding interactions with the substrate. In each case, the Ala mutant was made as a common null mutation, plus in some cases mutations that ablated the normal function but kept some of the character of the side chain. Mutagenesis was performed using the QuikChange system as described in Experimental Procedures, and all plasmids so produced were re-sequenced to ensure the fidelity of the mutation. Full-length proteins were expressed in, and purified from, *E. coli*, and each was characterized by PAGE analysis and ESI mass spectrometry. The masses were all consistent with the expected masses for such mutants (Table 1). The Q87M and N126A mutants were described earlier (*21*, *23*).

Kinetic parameters for hydrolysis of the *p*-nitrophenyl deoxy- and deoxyfluoro-β-xylobiosides by wild-type Cex are presented in Table 2, along with the calculated increase in

Table 1: Determination of the Molecular Weight of Cex and Mutants by Mass Spectrometry

enzyme	observed M_r (Da)	observed ΔM_r (Da)	expected ΔM_r (Da)
native Cex	47124 ± 3	0	0
Cex E43A	47064 ± 3	60 ± 5	58
Cex N44A	47082 ± 3	42 ± 5	43
Cex K47A	47070 ± 3	54 ± 5	57
Cex H80A	47058 ± 3	66 ± 5	66
Cex H80N	47100 ± 3	24 ± 5	23
Cex H80Q	47114 ± 3	10 ± 5	9

Table 2: Kinetic Parameters for the Hydrolysis of Deoxy/Deoxyfluoro Analogues by Wild-Type *C. fimi* Xylanase

	Michaelis−Menten kinetics			apparent binding energy contribution
substrate	k_{cat} (s^{-1})	K_m (mM)	k_{cat}/K_m ($s^{-1}\,mM^{-1}$)	$\Delta\Delta G^{\ddagger}$ (kcal mol^{-1})
$PNPX_2$	40 ± 2	0.017 ± 0.001	2300	0
2′H-$PNPX_2$	28 ± 2	1.4 ± 0.1	21	2.9
2′F-$PNPX_2$	nd[a]	nd[a]	74	2.1
3′H-$PNPX_2$	47 ± 2	0.42 ± 0.02	110	1.9
3′F-$PNPX_2$	48 ± 2	0.024 ± 0.002	2000	0.1
4′H-$PNPX_2$	32 ± 2	0.034 ± 0.002	930	0.6
4′F-$PNPX_2$	31 ± 2	0.015 ± 0.004	2100	0
3F-$PNPX_2$	0.006 ± 001	0.96 ± 0.04	0.006	7.9

[a] nd indicates that this kinetic parameter was not determined.

activation free energy for the glycosylation step associated with each substitution. This $\Delta\Delta G^{\ddagger}$ value was calculated from the ratios of the k_{cat}/K_m values of the parent substrate and the modified analogue according to the equation provided in Experimental Procedures.

Michaelis−Menten kinetic parameters for the hydrolysis of *p*-nitrophenyl xylobioside by each of the mutants of Cex are presented in Table 3. Also presented are values of k_{cat}/K_m independently measured using the substrate depletion method, wherever possible. As can be seen, the agreement between the two sets of data is excellent, confirming the validity of this approach for these studies. Again, the change in activation energy for the first (glycosylation) step associated with each mutation, calculated from relative k_{cat}/K_m values, is presented.

Kinetic parameters for the hydrolysis of the *p*-nitrophenyl deoxy- and deoxyfluoro-β-xylobiosides by Bcx are presented in Table 4. Because of the high K_m values exhibited by Bcx for aryl xylobioside substrates and the scarcity and low solubility of the modified xylobiosides, full Michaelis−Menten kinetic parameters could not be determined. Instead, values of k_{cat}/K_m for each substrate were determined by the substrate depletion method. These values are presented along with the calculated increase in activation free energy for the glycosylation step associated with each substitution.

DISCUSSION

As shown in Figures 2 and 3, which provide cartoons of the active sites of Cex and Bcx in their trapped 2-deoxy-2-fluoro-xylobiosyl−enzyme forms, recognition of the substrate and ultimately stabilization of the transition states are in each case achieved through a pre-organized set of networked hydrogen-bonding interactions. It is this set of hydrogen-bonding interactions that has been, site-selectively, compromised through modifications to the substrate or to the enzyme. Less evident in this cartoon but undoubtedly also of considerable importance is the set of van der Waals interactions between the nonpolar portions of the enzyme and the substrate. These structures will provide the basis for the subsequent discussion of the importance of hydrogen-bonding interactions in catalysis by Cex and Bcx. The discussion is broken down, in each case, into the importance of the interactions with the distal sugar (non-reducing end sugar), which occupies the −2 subsite of the enzyme, and of interactions with the proximal sugar, which occupies the −1 subsite.

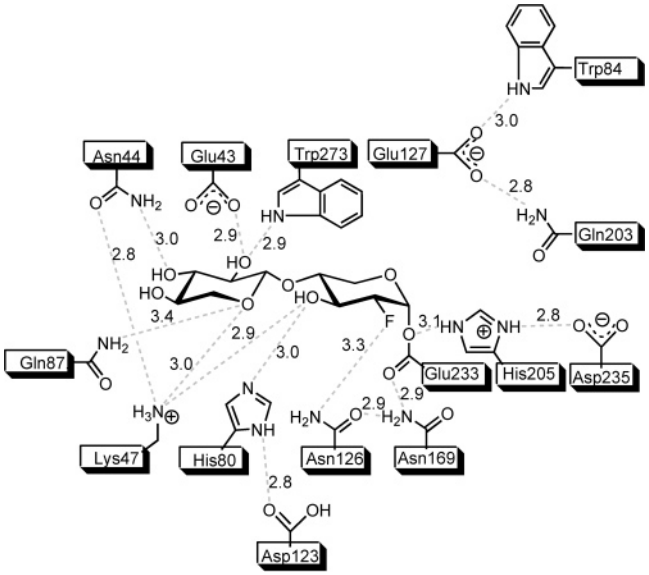

FIGURE 2: Scheme of protein−carbohydrate interactions in the active site region of the 2*F*-xylobiosyl−Cex-cd complex observed by 3D structural analysis (*21*). Hydrogen-bonding interactions between heteroatoms are in Angstroms. The distance between 2F and the carbonyl oxygen of Glu233 is 2.6 Å (not shown).

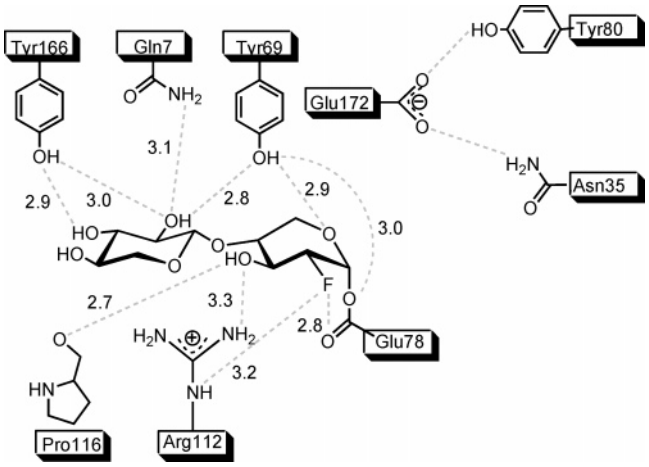

FIGURE 3: Scheme of protein−carbohydrate interactions in the active site region of the 2-fluoroxylobiosyl−Bcx complex observed by 3D structural analysis (*22*). Hydrogen-bonding interactions between heteroatoms are in Angstroms.

Previous kinetic studies on Cex have confirmed that the rate-limiting step in the reaction of Cex with *p*-nitrophenyl xylobioside is the hydrolysis of the xylobiosyl−enzyme intermediate: the deglycosylation step (*21*, *30*). Indeed the very low K_m value observed is consistent with this conclusion because it indicates substantial accumulation of the glyco-

Table 3: Kinetic Parameters for the Hydrolysis of $PNPX_2$ by Wild-Type and Mutant *C. fimi* Xylanase

	Michaelis−Menten kinetics			substrate depletion kinetics	apparent binding energy contribution
enzyme	k_{cat} (s^{-1})	K_m (mM)	k_{cat}/K_m ($s^{-1}\,mM^{-1}$)	k_{cat}/K_m ($s^{-1}\,mM^{-1}$)	$\Delta\Delta G^{\ddagger}$ (kcal mol^{-1})
native Cex	40 ± 2	0.017 ± 0.001	2300	2100 ± 200	0
Cex E43A	33 ± 2	5 ± 2	6.0	5.3 ± 0.5	3.7
Cex N44A	110 ± 5	4 ± 2	29	31 ± 3	2.7
Cex K47A	0.43 ± 0.02	10 ± 3	0.045	0.054 ± 0.005	6.7
Cex H80A	0.50 ± 0.03	0.59 ± 0.03	0.86	0.80 ± 0.08	4.9
Cex H80N	0.15 ± 0.01	0.099 ± 0.005	1.5	nd[a]	4.5
Cex H80Q	0.044 ± 0.002	0.061 ± 0.003	0.72	nd[a]	5.0
Cex Q87M	58 ± 3	0.12 ± 0.01	480	nd[a]	1.0
Cex N126A	3.5 ± 0.2	8 ± 3	0.45	0.49 ± 0.05	5.3

[a] nd indicates that this kinetic parameter was not determined.

Table 4: Kinetic Parameters for the Hydrolysis of Deoxy/Deoxyfluoro Analogues of $PNPX_2$ by Wild-Type *B. circulans* Xylanase

	substrate depletion kinetics	apparent binding energy contribution
substrate	k_{cat}/K_m ($s^{-1}\,mM^{-1}$)	$\Delta\Delta G^{\ddagger}$ (kcal mol^{-1})
$PNPX_2$	0.13 ± 0.01	0
2′H-$PNPX_2$	0.0012 ± 0.0001	2.9
2′F-$PNPX_2$	0.0035 ± 0.0004	2.2
3′H-$PNPX_2$	0.0046 ± 0.0005	2.1
3′F-$PNPX_2$	0.050 ± 0.005	0.6
4′H-$PNPX_2$	0.34 ± 0.03	−0.6
4′F-$PNPX_2$	0.41 ± 0.04	−0.7

syl−enzyme intermediate. Rate-limiting deglycosylation for the mutants has also been confirmed by also measuring kinetic parameters for the mutants with a substrate containing an aglycone of greater leaving group ability, namely, the 2,5-dinitrophenyl xylobioside (aglycone $pK_a = 5.15$ vs *p*-nitrophenol pK_a of 7.18). As shown in Table S1 in Supporting Information, with the exception of the K47A mutant, the k_{cat} values measured in each case are essentially the same as those measured for $PNPX_2$, indicating that the glycosylation step is not rate-limiting and that the deglycosylation step is most likely rate-limiting. This was substantiated by the biphasic nature of the Lineweaver−Burk plots seen at higher substrate concentration, associated with the greater rate of reaction due to transglycosylation onto a second substrate molecule acting as acceptor. Plots of this type have been carefully evaluated previously and shown to arise when deglycosylation is the rate-limiting step (*30*). By contrast, the parameter k_{cat}/K_m reflects the first irreversible step, in this case the formation of the glycosyl−enzyme intermediate. Therefore, by inspecting the effects of each substitution on these two kinetic parameters (k_{cat}/K_m − glycosylation; k_{cat} − deglycosylation), we can gain insight into the importance of the interactions at that site on each step in catalysis.

Interactions with the Distal (−2 Subsite) Sugar. It is then striking to note that, for those substrates modified in the distal sugar, there is essentially *no* effect of substitution upon k_{cat} (Table 2). This indicates that the deglycosylation step is insensitive to substitutions on the distal sugar ring. By contrast, distal substitution has very significant effects upon the glycosylation step as indicated by the k_{cat}/K_m values, with binding energy contributions from each hydroxyl ranging up to 2.9 kcal mol^{-1}. Very similar effects upon k_{cat}/K_m are seen for Bcx, with $\Delta\Delta G^{\ddagger}$ values ranging from −0.7 up to 2.9 kcal mol^{-1} (Table 4). Unfortunately, because of the relatively high K_m values exhibited by Bcx and the scarcity of substrate, it was not possible to obtain k_{cat} values and thus to probe effects upon the deglycosylation step.

Gratifyingly, exactly the same pattern is seen in the kinetic parameters determined for the hydrolysis of $PNPX_2$ by the mutants of Cex. When hydrogen bonds that are exclusively formed with the *distal* sugar are ablated (E43A; N44A; and Q87M) the k_{cat} values for hydrolysis of $PNPX_2$ are essentially unaffected (Table 3). However, the effects upon k_{cat}/K_m are substantial, ranging from 1.0 to 3.7 kcal mol^{-1}. Thus, again, the hydrogen bonds formed with the distal sugar are important for the glycosylation transition state but not for the deglycosylation transition state.

Interactions with the Proximal (−1 Subsite) Sugar. A different picture is seen when considering hydrogen bonds formed with the *proximal* sugar. In all mutants in which side chains interacting with the proximal sugar are modified (K47A; H80A; H80N; H80Q; and N126A), values of both k_{cat} and k_{cat}/K_m drop (Table 3). The largest effect is upon k_{cat}/K_m, with $\Delta\Delta G^{\ddagger}$ values ranging from 4.5 to 6.7 kcal mol^{-1}. Unfortunately, only a very limited data set is available for xylobioside substrates in which the proximal sugar has been modified, and as noted earlier, these data are complicated by inductive effects upon transition state stability. However, comparison of the data for 3F-$PNPX_2$ with that for $PNPX_2$ reveals that indeed both k_{cat} and k_{cat}/K_m are severely affected, with the transition state for glycosylation being destabilized by a massive 7.9 kcal mol^{-1}, while that for deglycosylation is destabilized by approximately 5.2 kcal mol^{-1}. Part of this destabilization is undoubtedly a consequence of inductive effects, for which a crude estimate of 1.2 kcal mol^{-1} can be drawn from spontaneous hydrolysis data on similarly modified glucosides (*12*), leaving approximately 6.7 and 4.0 kcal mol^{-1} as the contributions of hydrogen bonding at this position to the glycosylation and deglycosylation steps. Likewise, though difficult to evaluate, enormous effects upon k_{cat} are seen for the substitution of the 2-hydroxyl in the proximal ring by fluorine, this being the basis for the use of such reagents as mechanism-based inactivators. Unfortunately, data are not available to allow direct comparisons of

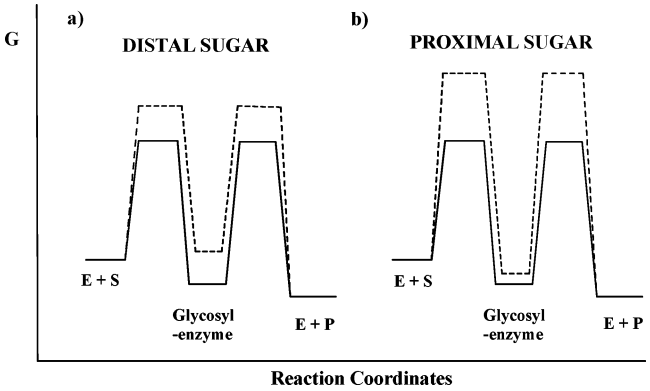

FIGURE 4: Reaction coordinate diagrams showing the consequences of modifications to the (a) distal sugar and (b) proximal sugar. The Gibbs free energy changes are shown for the wild-type enzyme (solid curve) and the mutants (dashed curve).

aryl xylobiosides with their 2-deoxy or 2-deoxy-2-fluoro analogues. However, a comparison of the k_i/K_i value for inactivation of Cex by 2,4-dinitrophenyl 2-deoxy−2-fluoro-β-cellobioside (2F-DNPC) with the k_{cat}/K_m for 2,4-dinitrophenyl β-cellobioside (DNPC) yields a $\Delta\Delta G^{\ddagger}$ of 5.8 kcal mol^{-1} for the glycosylation step (*30*). Effects on the deglycosylation step are much greater. Comparison of k_{cat} for DNPC (reflecting the deglycosylation step) with the reactivation rate constant for the 2-fluorocellobiosyl−enzyme results in a $\Delta\Delta G^{\ddagger}$ value of 11.3 kcal mol^{-1} (*30*), of which a part is undoubtedly due to inductive effects. However, even after correcting for this, a $\Delta\Delta G^{\ddagger}$ value of approximately 9 kcal mol^{-1} can be conservatively estimated for the contribution of the interactions at the 2-hydroxyl.

How then can these apparent effects on the two transition states be so different, especially in the case of interactions with the distal sugar, when, as a reasonable first assumption, the two transition states would be expected to be quite similar and to recruit similar binding interactions? The answer lies in considering the preceding ground states for each step. For data derived from k_{cat}/K_m values (glycosylation step), the preceding ground state is the free enzyme/free substrate. Consequently, $\Delta\Delta G^{\ddagger}$ values derived from this parameter are a measure of the strengths of interactions at that position in the glycosylation transition state relative to those formed with solvent. They are not, of course, measures of the full strength of the hydrogen-bonding interactions because that value is modulated by the strengths of those hydrogen bonds to water present in the free species that have to be broken upon complex formation, as described in detail elsewhere (*8*, *42*−*44*). By contrast, values derived from k_{cat} have, as their preceding ground state, the glycosyl−enzyme intermediate. Thus, $\Delta\Delta G^{\ddagger}$ values derived therefrom are *differences* in interaction energies between those formed in the intermediate and those formed at the transition state.

The implication of this, as illustrated in Figure 4, is that interactions formed with the distal sugar have the same strengths not only in the two transition states but also in the intervening glycosyl−enzyme intermediate. These interactions therefore fall into the category described by Albery and Knowles as "uniform binding interactions" (*1*, *45*). They form in the first Michaelis complex and are maintained with equal strength in all the intervening states along the reaction coordinate. Such interactions serve to improve k_{cat}/K_m, but have no positive effect whatsoever upon k_{cat}. By contrast, interactions with the proximal sugar are much stronger at the two transition states than in the intervening intermediate and thus fall into the category of "differential binding interactions" of Albery and Knowles (*1*, *45*). Interactions of this class are harder to recruit as they must become selectively stronger at the reaction transition state than in the ground state. They will necessarily exploit the bonding arrangements and charge distributions present at the transition state that differ from those in the ground state in order to achieve this selectivity.

These observations are, in fact, nicely consistent with the occurring chemistry because the *proximal* sugar undergoes substantial conformational rearrangement along the reaction coordinate to accommodate the planar oxocarbenium ion center formed at the transition state, most likely via a $^4H_3$ half-chair conformation in the case of Cex, as well as in acquiring and dispersing a partial positive charge (*46*). Interactions will have therefore evolved to be optimal at this transition state conformation. By contrast, no conformational changes are expected at the *distal* sugar; thus, differential recognition of the transition state would be very difficult. It therefore appears that Cex recruits both uniform binding interactions (at the distal sugar) and differential binding interactions (at the proximal sugar) in effecting catalysis on oligomeric substrates.

Interestingly, some indications of this behavior had been obtained in an earlier study of mechanisms of Cex-catalyzed hydrolysis of aryl cellobiosides and aryl glucosides (*30*). Brønsted plot analyses revealed that the rate-limiting step for the aryl glucosides was the glycosylation step, whereas that for the aryl cellobiosides was deglycosylation. Thus, the addition of a glucose residue to the substrate appears to selectively accelerate the glycosylation step, entirely consistent with the reaction coordinate diagrams in Figure 4. Further insight was obtained from the slopes of the two Brønsted plots derived from k_{cat}/K_m values, which reveal the charge development on the aglycone oxygen at the glycosylation transition state in each case. A slope of −1 for the *glucosides* indicated full negative charge development, while a slope of −0.3 for the *cellobiosides* revealed less charge development at the glycosylation transition state when both subsites are filled. This would be consistent with a more efficient catalytic system (less charge separation) and likely results from either or both of a greater degree of nucleophilic pre-association by the enzymatic nucleophile, Glu233, or a greater extent of proton donation from the acid catalyst, Glu127. The slightly lower alpha-deuterium kinetic isotope effect measured for the cellobiosides is consistent with this greater pre-association as at least one of the contributing factors. Our current study provides a much deeper understanding of the origin of this effect by showing that it is achieved through the recruitment of uniform binding interactions and by dissecting the contributions of each of the hydroxyl groups to that effect, as discussed below.

Contributions of Individual Interactions to Cex Catalysis. It is of interest to correlate the nature of the enzyme−substrate interactions, as observed crystallographically, with their strengths as, observed kinetically for the glycosylation transition state in this study. The strongest interactions with the distal sugar, 2.9 kcal mol^{-1}, are those seen at the 2′-position (deoxysugar data), and significantly, this is the only exclusive interaction that the distal sugar makes with a

charged partner (Figure 2). This is completely consistent with previous studies on other systems, which have suggested that charged hydrogen bonds contribute 3 kcal mol^{-1} or more to interaction energies of enzyme−ligand complexes (*8*, *44*). Because the 2′-hydroxyl must donate the hydrogen bond to the carboxylate of E43, the loss of almost all the interaction energy in the 2′-fluoro sugar case (2.1 kcal mol^{-1}) is also understandable because fluorine cannot donate a hydrogen bond. It could, however, still accept a hydrogen bond, if more weakly, from W272, hence the lower loss of interaction energy than was the case for the 2′-deoxy sugar (*47*−*50*).

When interaction strengths are considered on the basis of mutants of the enzyme at that locale, the somewhat greater loss of interaction energy (3.7 kcal mol^{-1}) for the E43A mutant is completely consistent with findings from the deoxy sugars studied. Presumably, other important protein−protein interactions (which can be equally important in transition state stabilization) are also lost, accounting for this slightly larger loss of stabilization energy. Hydrogen-bonding interactions of 1.9 kcal mol^{-1} at the 3′-position, as evidenced by the deoxy sugar data, are again quite consistent with earlier estimates of the values of hydrogen bonds between neutral partners being around 1.5 kcal mol^{-1}. However, in this case, the sugar hydroxyl is presumably acting as the hydrogen-bond acceptor from the amide nitrogen of N44 because the fluoro sugar exhibited essentially wild-type kinetic behavior. This would only be possible if the fluorine accepts the hydrogen bond. This polarity is also fully consistent with the observation of an interaction of the carbonyl oxygen of N44 with K47. Once again, deletion of the hydrogen bond through mutation (N44A) results in a slightly greater loss of interaction energy (2.7 kcal mol^{-1}), with the additional 0.8 kcal mol^{-1} presumably arising from the loss of that interaction of the amide carbonyl with the charged K47, *inter alia*. No significant hydrogen-bonding interactions are seen at the 4′-position of the distal sugar because further sugar residues are normally appended at this site in the intact xylan substrate. Again, consistently, the deoxy and deoxyfluoro sugars are turned over at essentially the same rates as that of the parent species.

The particularly important transition state hydrogen-bonding interactions at the 3-position of the proximal sugar inferred from kinetic parameters of the 3-deoxy-3-fluoroxylobioside (6.7 and 4.0 kcal mol^{-1} for the glycosylation and deglycosylation steps, respectively, after correction for inductive effects) arise from a pair of charged hydrogen-bonding interactions. These involve K47, recently unequivocally shown to be charged by ^{15}N NMR analysis of the trapped intermediate (*28*), and His80, also recently shown by ^{15}N NMR to be present in its charged, conjugate acid form in the free enzyme but to lose its proton upon the formation of the glycosyl−enzyme intermediate and accept a hydrogen bond from the 3-hydroxyl (Schubert et al., submitted for publication). Again, mutation of either of these residues is seen to have drastic effects on rates, as would be expected when a charged hydrogen-bonding network such as this is destroyed. Finally, removal of interactions at the 2-position of the proximal sugar either by mutation (N126A: $\Delta\Delta G^{\ddagger} = 5.3$ kcal mol^{-1}) or by fluorine substitution ($\Delta\Delta G^{\ddagger} = 5.8$ kcal mol^{-1}) enormously slows the glycosylation step. Because the principal transition state interaction at OH-2 is thought to be that with the carbonyl oxygen of the nucleophile (E233) itself, the value determined from N126A is only part of the story.

Contribution of Individual Interactions to Bcx Catalysis. A very similar picture emerges for Bcx when the data from Table 4 are analyzed. In this case, the 2′-hydroxyl of the distal sugar interacts with no less than three amino-acid residues, none of which are charged (Figure 3). Correspondingly, a 2.9 kcal mol^{-1} interaction is deduced from the 2′-deoxy substrate, consistent with three neutral hydrogen bonds, of which at least one must involve the 2′-hydroxyl as hydrogen bond acceptor, given that the 2′-deoxy-2′-fluoro sugar is a slightly better substrate than the corresponding 2′-deoxy sugar. Nevertheless, the deoxyfluoro sugar still loses 2.2 kcal mol^{-1} of interaction energy because of the loss of the donor hydrogen bond(s) at this position and the weakening of the other interactions.

The results with the 3′-deoxy and 3′-deoxyfluoro substrates suggest that the 3′-hydroxyl is involved primarily as an acceptor because the deoxyfluoro sugar is almost as good a substrate as the parent $PNPX_2$, whereas the 3′-deoxy sugar has lost 2.1 kcal mol^{-1} of interaction energy. This indicates that Tyr166 must donate a hydrogen bond to the 3′-hydroxyl.

Finally, once again, there is no hydrogen-bonding partner at the 4′-position because the substrate is normally extended through this position in the natural polymer. In this case, the 4′-modified substrates are in fact marginally better than the 4′-hydroxy parent. This is likely due to the fact that the 4′-hydroxyl of the parent substrate cannot form hydrogen bonds in the Michaelis complex that are as strong as those formed with water in the free state, and thus, binding is compromised. Such a loss of an interaction does not occur with the 4-deoxy sugar because it did not form hydrogen bonds at that position in the first place. Interestingly, similar findings were obtained in studies of oligosaccharyl fluoride substrates for human pancreatic α-amylase. Substrates in which the 4-hydroxyl group at the non-reducing end of the oligosaccharide was methylated were consistently better substrates, again presumably because there were no solution phase hydrogen-bonding partners that would be left unsatisfied at the transition state (*51*). Thus, while the dataset is less extensive in the case of Bcx, nonetheless a self-consistent pattern of hydrogen-bond polarities and strengths once again emerges between the crystallographic and the kinetic data.

CONCLUSIONS

A remarkably good agreement on the contributions of specific hydrogen-bonding interactions to catalysis by two different xylanases has therefore been found between the two different approaches employed: modification of the substrate to ablate the interaction or modification of the enzyme. The interaction strengths measured were consistent with the nature of the hydrogen bonds involved: charged or neutral. Particularly important was the demonstration, for the first time, of the recruitment of both uniform and differential binding interactions in the active site of a single enzyme. This provides a useful model for how exo-site activation is achieved in these and other enzymes such as proteases. No specific long-range conformational changes need to be invoked: a simple tethering effect is sufficient.

ACKNOWLEDGMENT

We thank Emily Kwan for technical assistance.

SUPPORTING INFORMATION AVAILABLE

Syntheses of the *p*-nitrophenyl deoxy- and deoxyfluoro-β-xylobiosides, and full characterizations. This material is available free of charge via the Internet at http://pubs.acs.org.

REFERENCES

1. Albery, W. J., and Knowles, J. R. (1976) Evolution of enzyme function and the development of catalytic efficiency, *Biochemistry 15*, 5631−5640.
2. Davies, G. J., Gloster, T. M., and Henrissat, B. (2005) Recent structural insights into the expanding world of carbohydrate-active enzymes, *Curr. Opin. Struct. Biol. 15*, 637−645.
3. Roeser, K. R., and Legler, G. (1981) Role of sugar hydroxyl groups in glycoside hydrolysis. Cleavage mechanism of deoxyglucosides and related substrates by β-glucosidase A3 from *Aspergillus wentii*, *Biochim. Biophys. Acta 657*, 321−333.
4. Namchuk, M. N., and Withers, S. G. (1995) Mechanism of *Agrobacterium* β-glucosidase: kinetic analysis of the role of noncovalent enzyme/substrate interactions, *Biochemistry 34*, 16194−16202.
5. Frandsen, T. P., Stoffer, B. B., Palcic, M. M., Hof, S., and Svensson, B. (1996) Structure and energetics of the glucoamylase-isomaltose transition-state complex probed by using modeling and deoxygenated substrates coupled with site-directed mutagenesis, *J. Mol. Biol. 263*, 79−89.
6. Sierks, M. R., and Svensson, B. (2000) Energetic and mechanistic studies of glucoamylase using molecular recognition of maltose OH groups coupled with site-directed mutagenesis, *Biochemistry 39*, 8585−8592.
7. McCarter, J. D., Adam, M. J., and Withers, S. G. (1992) Binding energy and catalysis. Fluorinated and deoxygenated glycosides as mechanistic probes of *Escherichia coli* (*lac*Z) β-galactosidase, *Biochem. J. 286*, 721−727.
8. Street, I. P., Armstrong, C. R., and Withers, S. G. (1986) Hydrogen bonding and specificity. Fluorodeoxy sugars as probes of hydrogen bonding in the glycogen phosphorylase-glucose complex, *Biochemistry 25*, 6021−6027.
9. Street, I. P., Rupitz, K., and Withers, S. G. (1989) Fluorinated and deoxygenated substrates as probes of transition-state structure in glycogen phosphorylase, *Biochemistry 28*, 1581−1587.
10. Withers, S. G., and Rupitz, K. (1990) Measurement of active-site homology between potato and rabbit muscle α-glucan phosphorylases through use of a linear free energy relationship, *Biochemistry 29*, 6405−6409.
11. Eis, C., and Nidetzky, B. (2002) Substrate-binding recognition and specificity of trehalose phosphorylase from *Schizophyllum commune* examined in steady-state kinetic studies with deoxy and deoxyfluoro substrate analogues and inhibitors, *Biochem. J. 363*, 335−340.
12. Namchuk, M. N., McCarter, J. D., Becalski, A., Andrews, T., and Withers, S. G. (2000) The role of sugar substituents in glycoside hydrolysis, *J. Am. Chem. Soc. 122*, 1270−1277.
13. Percival, M. D., and Withers, S. G. (1992) Binding energy and catalysis: deoxyfluoro sugars as probes of hydrogen bonding in phosphoglucomutase, *Biochemistry 31*, 498−505.
14. Piotukh, K., Serra, V., Borriss, R., and Planas, A. (1999) Protein-carbohydrate interactions defining substrate specificity in *Bacillus* 1,3-1,4-β-D-glucan 4-glucanohydrolases as dissected by mutational analysis, *Biochemistry 38*, 16092−16104.
15. Gaiser, O. J., Piotukh, K., Ponnuswamy, M. N., Planas, A., Borriss, R., and Heinemann, U. (2006) Structural basis for the substrate specificity of a *Bacillus* 1,3-1,4-β-glucanase, *J. Mol. Biol. 357*, 1211−1225.
16. Zechel, D. L., and Withers, S. G. (2000) Glycosidase mechanisms: anatomy of a finely tuned catalyst, *Acc. Chem. Res. 33*, 11−18.
17. White, A., Withers, S. G., Gilkes, N. R., and Rose, D. R. (1994) Crystal structure of the catalytic domain of the β-1,4-glycanase Cex from *Cellulomonas fimi*, *Biochemistry 33*, 12546−12552.
18. White, A., Tull, D., Johns, K., Withers, S. G., and Rose, D. R. (1996) Crystallographic observation of a covalent catalytic intermediate in a β-glycosidase, *Nat. Struct. Biol. 3*, 149−154.
19. Wakarchuk, W. W., Campbell, R. L., Sung, W. L., Davoodi, J., and Yaguchi, M. (1994) Mutational and crystallographic analyses of the active site residues of the *Bacillus circulans* xylanase, *Protein Sci. 3*, 467−475.
20. Notenboom, V., Birsan, C., Nitz, M., Rose, D. R., Warren, R. A. J., and Withers, S. G. (1998) Insights into transition state stabilization of the β-1,4-glycosidase Cex by covalent intermediate accumulation in active site mutants, *Nat. Struct. Biol. 5*, 812−818.
21. Notenboom, V., Birsan, C., Warren, R. A. J., Withers, S. G., and Rose, D. R. (1998) Exploring the cellulose/xylan specificity of the β-1,4-glycanase Cex from *Cellulomonas fimi* through crystallography and mutation, *Biochemistry 37*, 4751−4758.
22. Sidhu, G., Withers, S. G., Nguyen, N. T., McIntosh, L. P., Ziser, L., and Brayer, G. D. (1999) Sugar ring distortion in the glycosyl-enzyme intermediate of a family G/11 xylanase, *Biochemistry 38*, 5346−5354.
23. Williams, S. J., Notenboom, V., Wicki, J., Rose, D. R., and Withers, S. G. (2000) A new, simple, high-affinity glycosidase inhibitor: analysis of binding through X-ray crystallography, mutagenesis, and kinetic analysis, *J. Am. Chem. Soc. 122*, 4229−4230.
24. Williams, S. J., Hoos, R., and Withers, S. G. (2000) Nanomolar versus millimolar inhibition by xylobiose-derived azasugars: significant differences between two structurally distinct xylanases, *J. Am. Chem. Soc. 122*, 2223−2235.
25. Notenboom, V., Williams, S. J., Hoos, R., Withers, S. G., and Rose, D. R. (2000) Detailed structural analysis of glycosidase/inhibitor interactions: complexes of Cex from *Cellulomonas fimi* with xylobiose-derived aza-sugars, *Biochemistry 39*, 11553−11563.
26. McIntosh, L. P., Hand, G., Johnson, P. E., Joshi, M. D., Körner, M., Plesniak, L. A., Ziser, L., Wakarchuk, W. W., and Withers, S. G. (1996) The pK_a of the general acid/base carboxyl group of a glycosidase cycles during catalysis: a ^{13}C-NMR study of *Bacillus circulans* xylanase, *Biochemistry 35*, 9958−9966.
27. Plesniak, L. A., Connelly, G. P., Wakarchuk, W. W., and McIntosh, L. P. (1996) Characterization of a buried neutral histidine residue in *Bacillus circulans* xylanase: NMR assignments, pH titration, and hydrogen exchange, *Protein Sci. 5*, 2319−2328.
28. Poon, D. K. Y., Schubert, M., Au, J., Okon, M., Withers, S. G., and McIntosh, L. P. (2006) Unambiguous determination of the ionization state of a glycoside hydrolase active site lysine by ^{1}H-^{15}N heteronuclear correlation spectroscopy, *J. Am. Chem. Soc. 128*, 15388−15389.
29. Connelly, G. P., Withers, S. G., and McIntosh, L. P. (2000) Analysis of the dynamic properties of *Bacillus circulans* xylanase upon formation of a covalent glycosyl-enzyme intermediate, *Protein Sci. 9*, 512−524.
30. Tull, D., and Withers, S. G. (1994) Mechanisms of cellulases and xylanases: a detailed kinetic study of the exo-β-1,4-glycanase from *Cellulomonas fimi*, *Biochemistry 33*, 6363−6370.
31. Ziser, L., Setyawati, I., and Withers, S. G. (1995) Syntheses and testing of substrates and mechanism-based inactivators for xylanases, *Carbohydr. Res. 274*, 137−153.
32. Charnock, S. J., Spurway, T. D., Xie, H., Beylot, M.-H., Virden, R., Warren, R. A. J., Hazlewood, G. P., and Gilbert, H. J. (1998) The topology of the substrate binding clefts of glycosyl hydrolase family 10 xylanases are not conserved, *J. Biol. Chem. 273*, 32187−32199.
33. Lawson, S. L., Wakarchuk, W. W., and Withers, S. G. (1996) Effects of both shortening and lengthening the active site nucleophile of *Bacillus circulans* xylanase on catalytic activity, *Biochemistry 35*, 10110−10118.
34. Lawson, S. L., Wakarchuk, W. W., and Withers, S. G. (1997) Positioning the acid/base catalyst in a glycosidase: studies with *Bacillus circulans* xylanase, *Biochemistry 36*, 2257−2265.
35. MacLeod, A. M., Lindhorst, T., Withers, S. G., and Warren, R. A. J. (1994) The acid/base catalyst in the exoglucanase/xylanase from *Cellulomonas fimi* is glutamic acid 127: evidence from detailed kinetic studies of mutants, *Biochemistry 33*, 6371−6376.
36. MacLeod, A. M., Tull, D., Rupitz, K., Warren, R. A. J., and Withers, S. G. (1996) Mechanistic consequences of mutation of

active site carboxylates in a retaining β-1,4-glycanase from *Cellulomonas fimi*, *Biochemistry 35*, 13165−13172.
37. Andrews, S. R., Charnock, S. J., Lakey, J. H., Davies, G. J., Claeyssens, M., Nerinckx, W., Underwood, M., Sinnott, M. L., Warren, R. A. J., and Gilbert, H. J. (2000) Substrate specificity in glycoside hydrolase family 10. Tyrosine 87 and leucine 314 play a pivotal role in discriminating between glucose and xylose binding in the proximal active site of *Pseudomonas cellulosa* xylanase 10A, *J. Biol. Chem. 275*, 23027−23033.
38. O'Neill, G., Goh, S. H., Warren, R. A. J., Kilburn, D. G., and Miller, R. C., Jr. (1986) Structure of the gene encoding the exoglucanase of *Cellulomonas fimi*, *Gene 44*, 325−330.
39. Sung, W. L., Luk, C. K., Zahab, D. M., and Wakarchuk, W. (1993) Overexpression of the *Bacillus subtilis* and *circulans* xylanases in *Escherichia coli*, *Protein Expression Purif. 4*, 200−206.
40. Leatherbarrow, R. J. (1989) *GraFit*, Version 4.0, Erithacus Software Limited, Surrey, U.K.
41. Ziser, L., and Withers, S. G. (1994) A short synthesis of β-xylobiosides, *Carbohydr. Res. 265*, 9−17.
42. Jencks, W. P. (1975) Binding energy, specificity, and enzymic catalysis: the Circe effect, *Adv. Enzymol. Relat. Areas Mol. Biol. 43*, 219−410.
43. Fersht, A. R., Shi, J. P., Knill-Jones, J., Lowe, D. M., Wilkinson, A. J., Blow, D. M., Brick, P., Carter, P., Waye, M. M. Y., and Winter, G. (1985) Hydrogen bonding and biological specificity analysed by protein engineering, *Nature 314*, 235−238.
44. Fersht, A. R. (1987) Dissection of the structure and activity of the tyrosyl-tRNA synthetase by site-directed mutagenesis, *Biochemistry 26*, 8031−8037.
45. Fersht, A. (1999) *Structure and Mechanism in Protein Science: A Guide to Enzyme Catalysis and Protein Folding*, W. H. Freeman and Company, New York.
46. Money, V. A., Smith, N. L., Scaffidi, A., Stick, R. V., Gilbert, H. J., and Davies, G. J. (2006) Substrate distortion by a lichenase highlights the different conformational itineraries harnessed by related glycoside hydrolases, *Angew. Chem., Int. Ed. 45*, 5136−5140.
47. Carosati, E., Sciabola, S., and Cruciani, G. (2004) Hydrogen bonding interactions of covalently bonded fluorine atoms: from crystallographic data to a new angular function in the GRID force field, *J. Med. Chem. 47*, 5114−5125.
48. Brammer, L., Bruton, E. A., and Sherwood, P. (2001) Understanding the behavior of halogens as hydrogen bond acceptors, *Cryst. Growth Des. 1*, 277−290.
49. Howard, J. A. K., Hoy, V. J., O'Hagan, D., and Smith, G. T. (1996) How good is fluorine as a hydrogen bond acceptor? *Tetrahedron 52*, 12613−12622.
50. Shimoni, L., and Glusker, J. P. (1994) The geometry of intermolecular interactions in some crystalline fluorine-containing organic compounds, *Struct. Chem. 5*, 383−397.
51. Damager, I., Numao, S., Chen, H., Brayer, G. D., and Withers, S. G. (2004) Synthesis and characterisation of novel chromogenic substrates for human pancreatic α-amylase, *Carbohydr. Res. 339*, 1727−1737.

BI700359E